Supplementary material for Seismic waveform tomography of the Central and Eastern Mediterranean upper mantle

Nienke Blom, Alexey Gokhberg, Andreas Fichtner

September 17, 2019

In this Supplementary material, we report the events used in the inversion (Section 1), the adaptations made to the parameters of certain events (Section 2) and the processing applied to raw gradients in the inversion as well as the processing applied to cumulative updates after some sets of iterations (Section 3). Separate to this document, we provide a video of a 3-D visualisation of the final model, as well as the vtk and ParaView files corresponding to this.

1 List of events used in the inversion

Table 1 contains all events used in the inversion. Events whose parameters were shifted are included in the table twice: once with the original parameters (from the CMT catalogue, Ekström et al., 2012; Dziewonski et al., 1981, http://www.globalcmt.org) and once with adapted parameters. Original events are marked with a star (*), adapted events are italicised. The final column gives the iterations in which each of the events were used.

The new events that are used to test the final model and which are not used in the inversion are included at the end of the table below a double horizontal line. Letters A–E correspond to the letters A–E in Figure 14 in the manuscript.

	Origin time (UTC)	Latitude [°]	Longitude [°]	Depth [km]	Magnitude [Mwc]	Iterations
event_01	2014-05-24 09:25:18	40.30	25.67	12.0	6.90	0–100
event_03	2000-06-15 21:30:36	34.45	20.49	15.0	5.10	0–19
event_04	2013-06-16 21:39:07	34.22	25.19	20.0	6.10	0–100
event_06	2012-10-19 03:35:14	32.44	31.02	29.0	5.00	0–100
event_07	2010-11-14 23:08:28	36.48	36.08	12.0	4.90	0–100
event_08	2008-02-15 10:36:21	33.27	35.32	12.1	5.10	0–100
event_09	2010-11-03 00:57:00	43.67	20.65	13.8	5.50	0–100
event_12	2000-06-06 02:41:52	40.75	32.70	15.0	6.00	0–100
event_14	2009-12-29 11:08:56	32.56	15.04	12.0	5.00	0–100
event_16	2015-10-09 14:39:19	40.80	36.62	17.8	5.00	0–100
event_19	2012-04-26 22:05:34	39.09	29.25	13.6	4.80	0–100
event_24	2009-05-24 16:17:53	41.17	22.79	12.8	5.30	0–100
event_25	2014-11-07 17:13:01	38.15	22.12	13.2	5.10	0–100
event_29	1998-05-28 18:33:33	31.39	27.36	39.0	5.50	0–19
event_31	2015-04-15 08:25:15	34.72	32.36	17.9	5.30	0–100
event_32	2002-09-06 01:21:33	38.42	13.57	15.0	5.90	0–65
event_33 *	2009-04-06 01:32:49	42.29	13.35	12.0	6.30	0–28
event_33_shift	***2009-04-06 01:32:46***	*42.29*	*13.35*	*12.0*	*6.30*	*30–100*
event_34	2008-02-14 10:09:29	36.24	21.79	20.0	6.80	0–100
event_35	2009-09-06 21:49:46	41.37	20.36	12.0	5.50	0–100
event_36	2013-10-12 13:11:56	35.37	23.37	15.0	6.80	0–100
event_37	2015-11-17 07:10:12	38.47	20.53	15.0	6.50	0–100
event_38 *	2012-06-10 12:44:19	36.28	29.06	28.4	6.10	0–65
event_38_shift	*2012-06-10 12:44:19*	***36.34***	***29.00***	*28.4*	*6.10*	*65–100*
event_39	2002-02-03 07:11:43	38.62	31.21	15.0	6.50	0–19
event_40	2010-03-08 02:32:37	38.82	40.04	15.1	6.10	0–100
event_41	2015-06-27 15:34:03	28.83	34.62	28.3	5.60	0–100
event_42	2012-05-22 00:00:33	42.51	23.05	12.8	5.60	0–100
event_43	2002-11-01 15:09:09	41.80	14.88	15.0	5.70	0–85

Continued on next page

	Origin time (UTC)	Latitude [°]	Longitude [°]	Depth [km]	Magnitude [Mwc]	Iterations
event_44	2003-03-29 17:42:21	42.89	15.22	15.0	5.50	0–85
event_45	2004-02-11 08:15:06	31.62	35.31	26.1	5.30	0–100
event_46	2012-05-11 18:48:32	34.22	34.17	25.5	5.30	0–100
event_47	2001-06-25 13:28:52	37.23	35.71	15.0	5.40	0–19
event_48	2008-11-12 14:03:21	38.92	35.46	17.0	5.10	0–100
event_49	2003-07-13 01:48:25	38.16	38.90	15.0	5.50	0–85
event_50	2002-06-24 01:20:42	36.03	10.29	15.0	5.20	0–65
event_51	2011-07-07 19:21:50	41.94	7.63	13.3	5.10	0–100
event_53	2010-11-03 18:13:13	39.95	12.89	491.8	5.20	0–19
event_54	2012-05-20 02:03:56	44.89	11.44	12.0	6.10	0–65
event_55	2009-08-05 07:49:04	43.42	28.60	19.9	5.00	0–100
event_56	2012-03-26 10:35:35	39.15	42.20	19.5	5.20	0–100
event_57	2007-01-21 07:39:01	39.60	42.72	14.7	5.10	0–100
event_58	2012-10-25 23:05:28	39.88	15.98	12.0	5.30	0–100
event_59	2009-11-03 05:25:13	37.35	20.19	15.5	5.80	0–100
event_61	2007-08-31 20:52:45	36.59	26.32	15.7	5.20	0–100
event_62	2016-08-24 02:33:32	42.68	13.15	12.0	5.60	0–100
event_63	2007-11-09 01:43:09	38.78	25.66	15.2	5.18	0–100
event_64	2008-08-03 00:39:19	39.54	23.76	12.0	5.25	0–100
event_65	2005-10-17 05:45:24	38.21	26.59	15.2	5.48	0–100
event_66	2013-01-08 14:16:11	39.62	25.61	14.6	5.81	0–100
event_67	2009-08-21 13:40:01	41.76	19.07	21.1	5.06	0–100
event_68	2013-07-21 01:32:27	43.48	13.68	12.0	5.11	0–100
event_69	2006-05-25 23:14:41	36.55	19.91	23.5	5.19	0–100
event_70	2007-02-03 13:43:25	35.67	22.39	53.5	5.40	0–100
event_71	2008-06-12 00:20:49	35.28	26.36	40.7	5.13	0–100
event_72	2011-05-19 20:39:05	34.32	23.66	17.8	5.24	0–100
event_73	2012-01-27 01:33:25	35.89	24.88	15.6	5.42	0–100
event_74	2005-01-11 04:35:57	36.84	27.84	12.2	5.03	0–19
event_75	2007-05-21 16:39:11	35.14	27.62	18.1	5.03	0–100
event_76	2007-12-20 09:48:32	39.43	33.10	12.0	5.66	0–100
event_77	2011-09-22 03:22:38	39.68	38.60	16.1	5.56	0–85
event_78	2005-06-06 07:41:33	39.44	40.87	15.4	5.64	0–85
event_79	2007-10-29 09:23:19	36.89	29.21	12.0	5.30	0–100
event_80	2015-11-29 00:28:11	38.82	37.75	20.2	5.11	0–100
event_81	2014-08-24 19:43:39	37.64	30.61	18.1	5.09	0–100
event_82	2011-07-25 17:57:22	40.80	27.72	12.0	5.09	0–100
event_83	2012-09-19 09:17:48	37.28	37.12	21.4	5.04	0–100
event_84	2006-10-24 14:00:23	40.46	28.98	14.3	5.05	0–100
event_85	2008-01-06 05:14:23	36.98	22.87	92.4	6.17	0–100
event_86	2014-08-29 03:45:08	36.46	23.62	100.2	5.81	0–100
event_87	2014-04-04 20:08:08	37.11	23.69	122.4	5.59	0–100
event_88	2008-06-18 01:58:45	37.63	22.78	92.5	5.06	0–100
event_89	2007-10-27 05:29:43	37.70	21.33	27.5	5.11	0–100
event_90	2006-10-26 14:28:39	38.65	15.41	216.8	5.79	0–100
event_91	2005-07-10 13:10:15	42.37	19.70	12.0	5.15	0–100
event_92	2005-09-27 00:25:39	43.18	18.18	29.9	5.09	0–100
event_93	2013-06-21 10:34:00	44.10	10.17	12.0	5.32	0–100
event_94	2015-06-09 01:09:06	38.51	23.43	12.6	5.28	0–100
event_95	2007-04-10 10:41:05	38.55	21.48	12.0	5.16	0–85
event_96	2013-07-02 10:45:23	39.97	21.74	28.0	5.06	0–100
event_97	2007-06-29 18:09:15	39.19	20.11	12.0	5.43	0–100
event_98 *	2013-12-28 15:21:06	35.82	30.97	52.6	5.93	0–65
event_98_shift	*2013-12-28 15:21:06*	***35.97***	***31.22***	*52.6*	*5.93*	*65–100*
event_99	2012-07-09 13:55:00	35.36	28.96	71.2	5.74	0–100
event_100	2016-10-30 06:40:24	42.75	13.16	12.0	6.60	10–100
event_101*	2016-08-24 01:36:36	42.64	13.22	12.0	6.20	10–65

Continued on next page

	Origin time (UTC)	Latitude [°]	Longitude [°]	Depth [km]	Magnitude [Mwc]	Iterations
event_101_shift	***2016-08-24 01:36:37***	*42.64*	*13.22*	*12.0*	*6.20*	*65–100*
event_102 (D)	2017-07-20 22:31:17	36.80	27.62	12.0	6.60	
event_104 (C)	2017-06-12 12:28:41	38.81	26.32	12.0	6.40	
event_105	2017-03-02 11:07:27	37.53	38.45	17.2	5.60	
event_106 (B)	2018-01-04 10:46:12	42.60	19.82	14.7	5.20	
event_107 (A)	2017-01-18 10:14:14	42.48	13.28	12.0	5.70	
event_109 (E)	2016-05-16 01:45:59	28.45	34.58	15.0	5.30	

2 Adapted event parameters

Below, we discuss the changes that were made to certain event parameters, including the rationale behind these changes. The actual parameters are given in Table 1 above.

Event 33

In practically all seismograms, a static shift between observed and synthetic traces is observed (Figure 1). This is independent from epicentral distance and is visible on all components. It is confirmed by the spatial distribution of phase shifts, and the skewed histogram of phase shifts as demonstrated in Figure 2. A time shift of 3 seconds was applied to remove this static shift. As a result, the phase shifts centre around a roughly zero mean (Figure 3).

A time shift is not the only way in which the shift can be explained; however, for the purposes of the inversion (and given the additional constraints given by other events in the area) it is the easiest and most workable explanation.

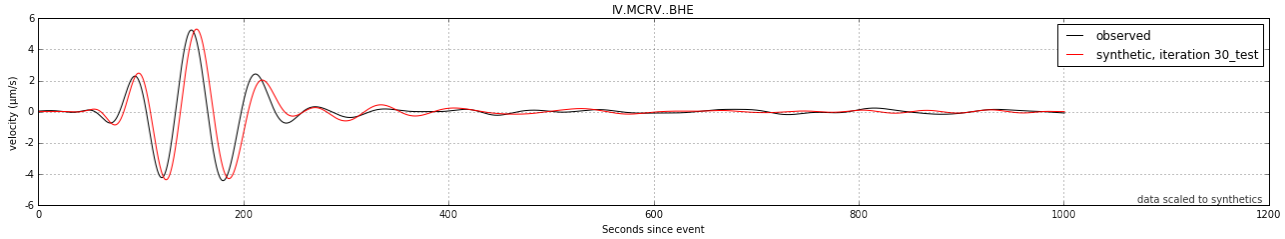

(a) Station IV.MCRV (E component).

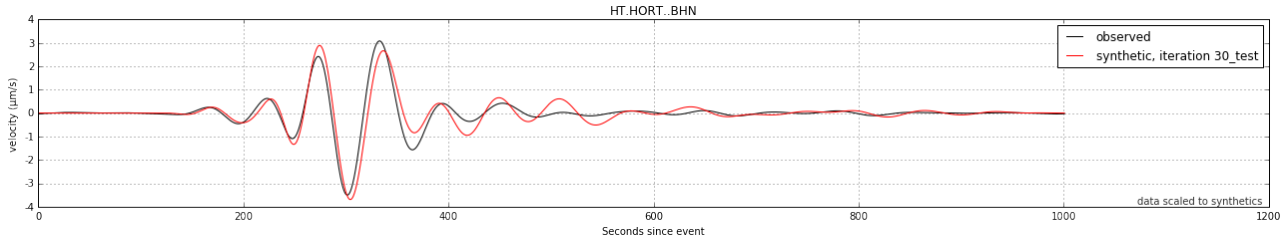

(b) Station HT.HORT (N component).

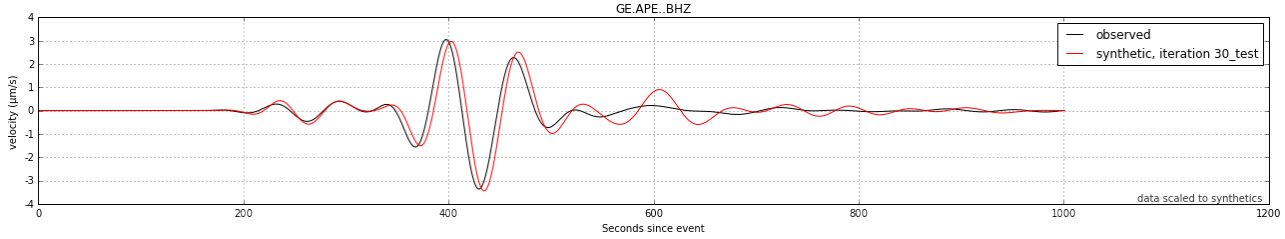

(c) Station GE.APE (Z component).

Figure 1: Seismograms for event 33 (uncorrected) and iteration 30 (55–150 s).

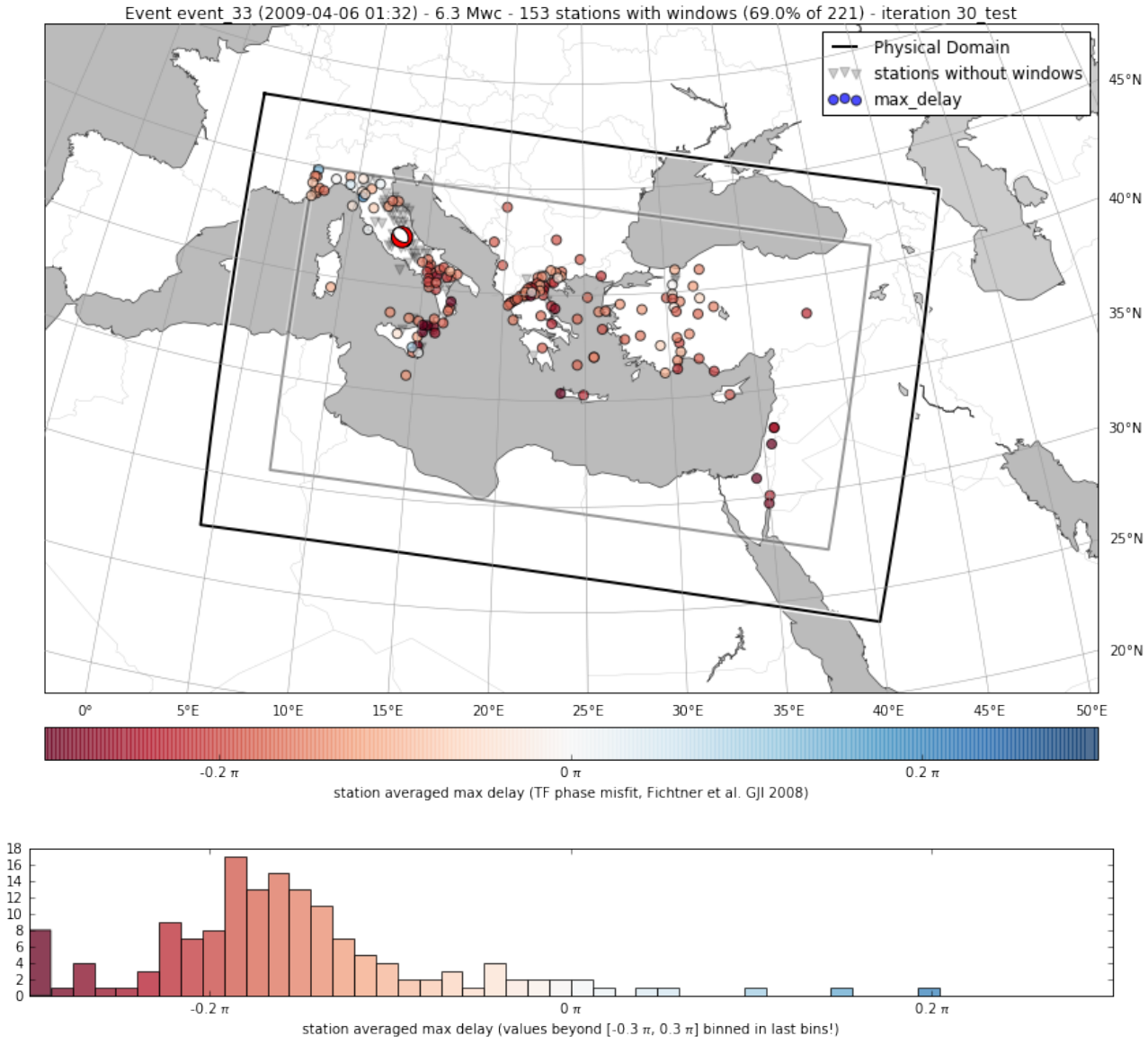

Figure 2: Original distribution of "max delay" phase shifts for event 33 at iteration 30 (55–150 s). This value is computed for each window as $\max(W_p\,(\phi - \phi_{\text{obs.}}))$ – see Equation 2 in the manuscript.

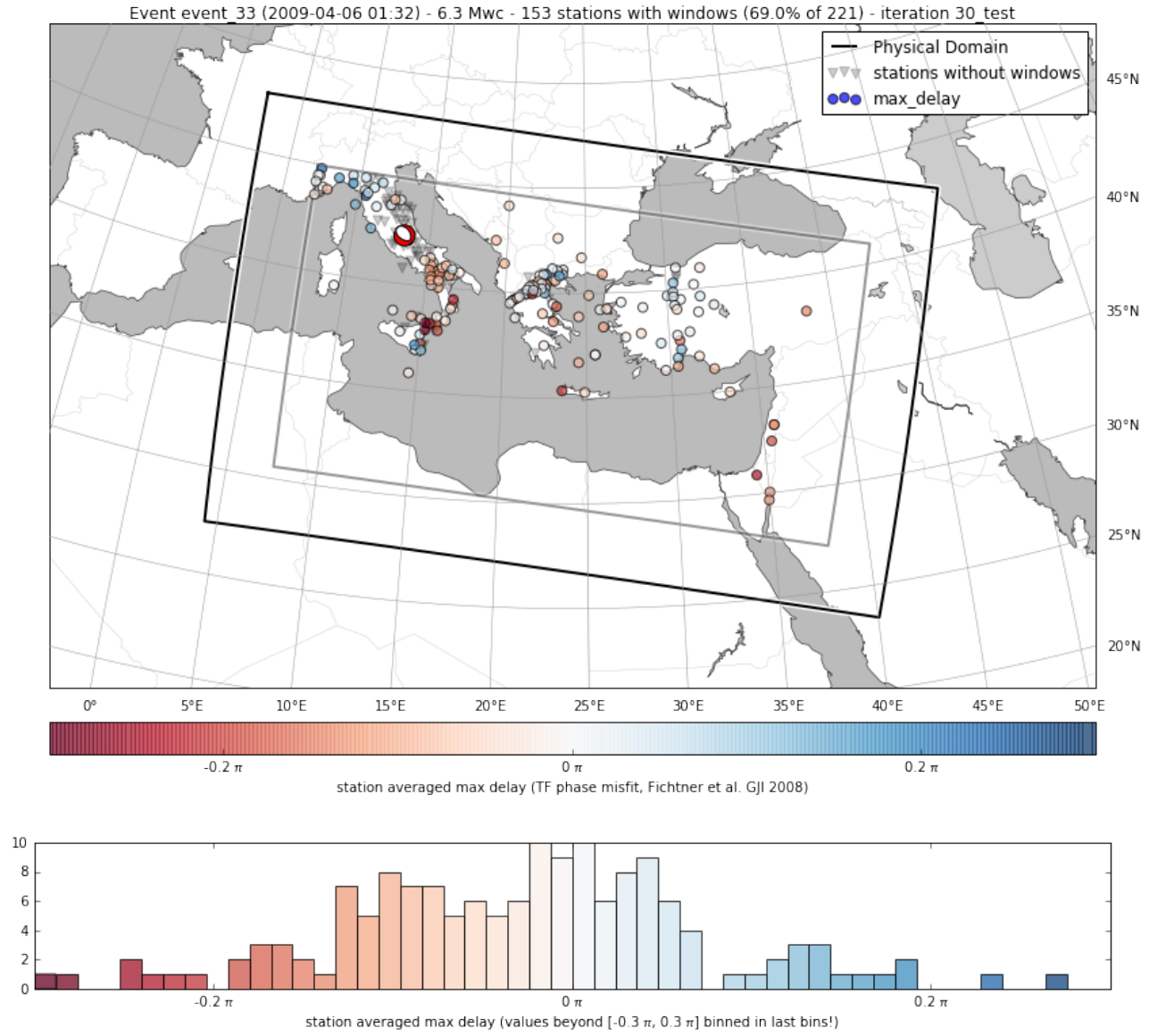

Figure 3: Distribution of "max delay" phase shifts for event 33 at iteration 30 (55–150 s) after shifting the event origin time by 3 seconds forward.

Event 38

Event 38 shows a geographical pattern of phase shifts, with positive shifts towards the north-west and negative shifts towards the south-east (Figure 4). Such phase shifts were not encountered for other events in the same area. This geographical pattern is therefore most easily explained using a small shift of the event towards the north-west. As a result of the applied shift in location, the spatial pattern of space shifts didappears and the histogram of phase shifts centres more around zero (Figure 5). The new location also corresponds more closely with the reported ISC-EHB location (Engdahl et al., 1998; Weston et al., 2018).

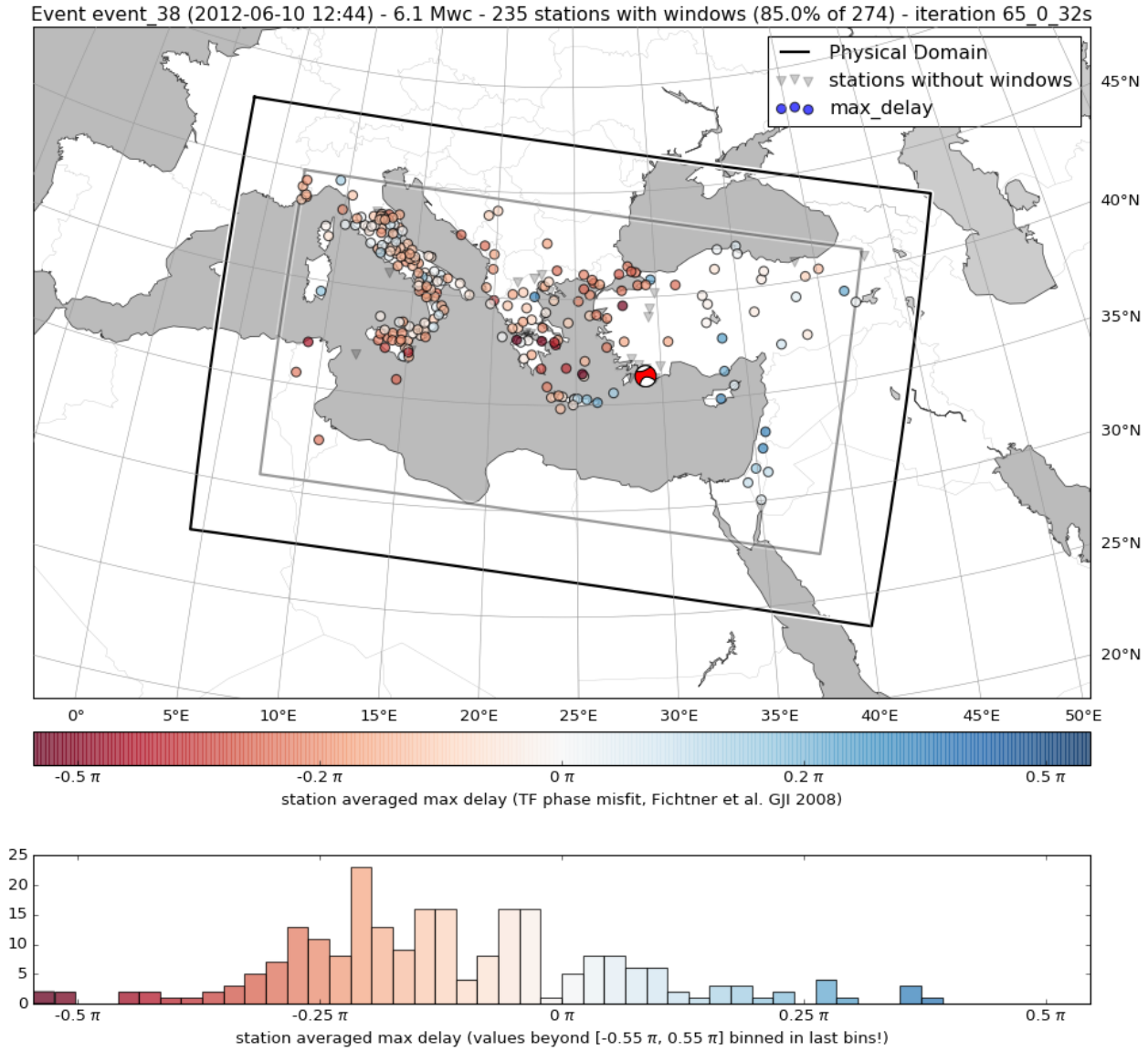

Figure 4: Original distribution of "max delay" phase shifts for event 38 at iteration 65 (32–150 s).

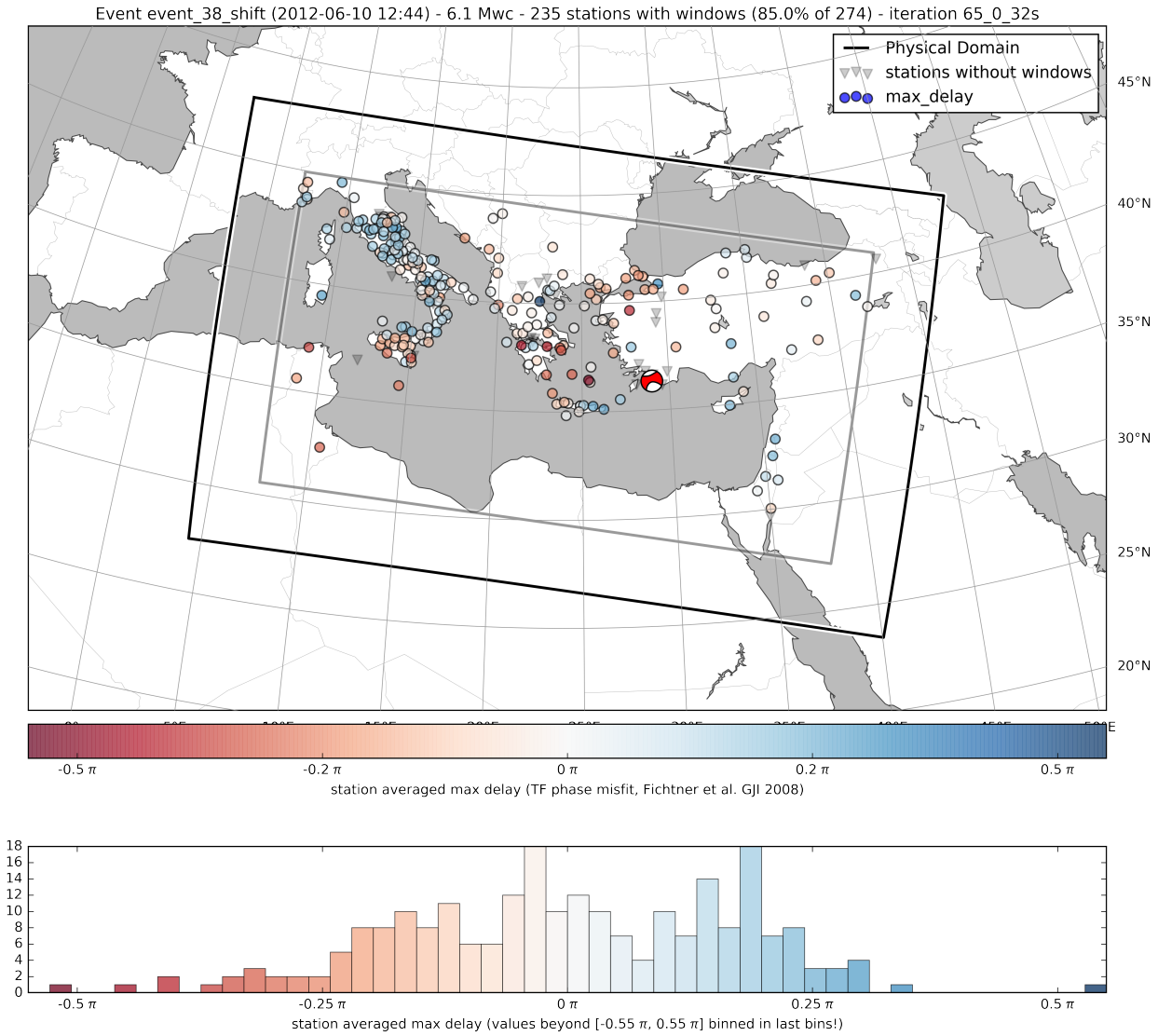

Figure 5: Distribution of "max delay" phase shifts for event 38 at iteration 65 (32–150 s) after shifting the event location towards the north-east (latitude + 0.06°, longitude - 0.06°).

Event 98

Event 98 shows a strong geographical pattern of phase shifts, with positive shifts towards the south-west and negative shifts towards the north-east (Figure 6). Such phase shifts were not encountered for other events in the same area. This geographical pattern is therefore most easily explained using a relocation of the event towards the north-east. As a result of this, the spatial pattern disappears entirely and the histogram becomes more unimodal and centering around zero (Figure 7). The new location also corresponds more closely with the reported ISC-EHB location (Engdahl et al., 1998; Weston et al., 2018).

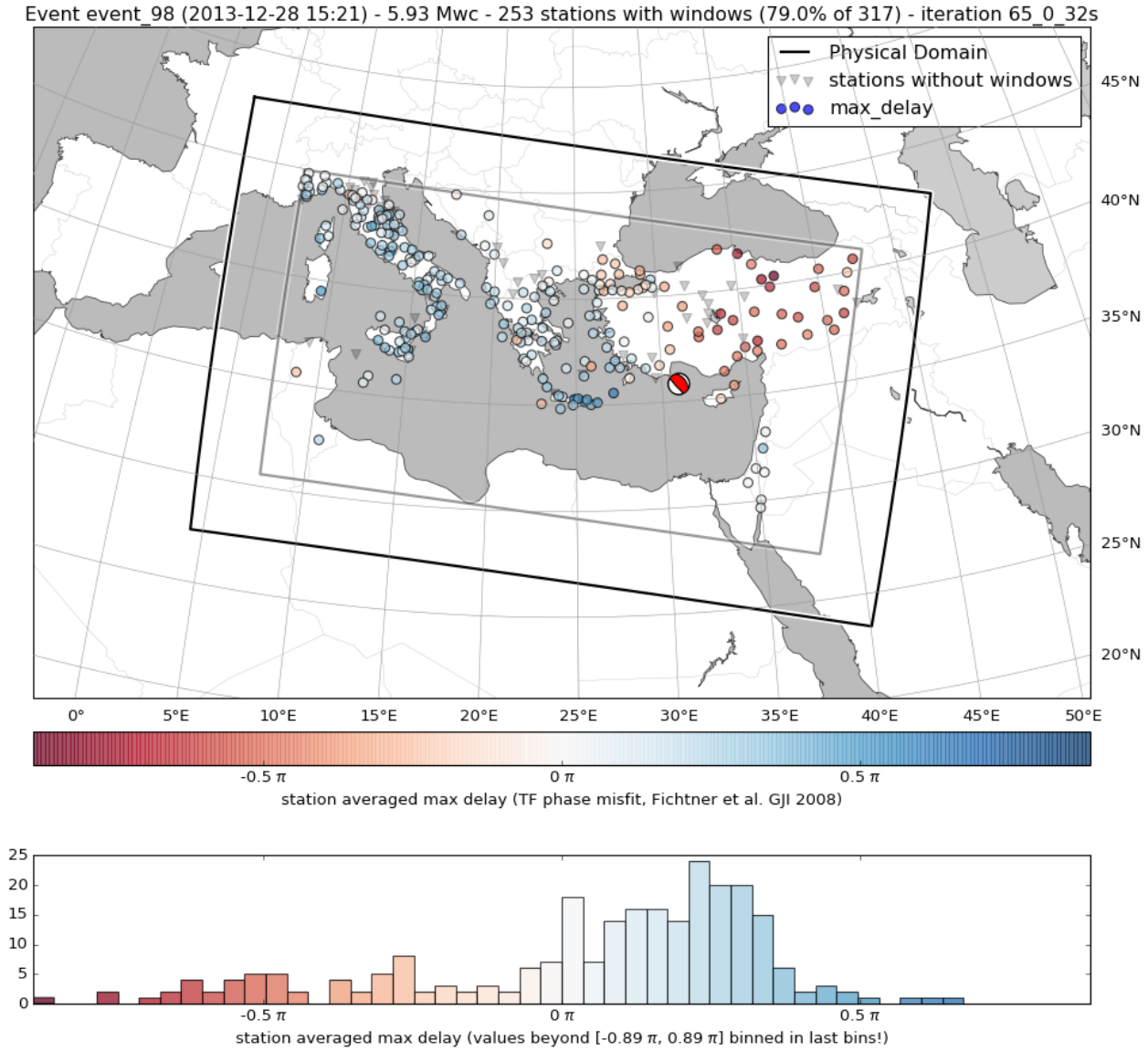

Figure 6: Original distribution of "max delay" phase shifts for event 98 at iteration 65 (32–150 s).

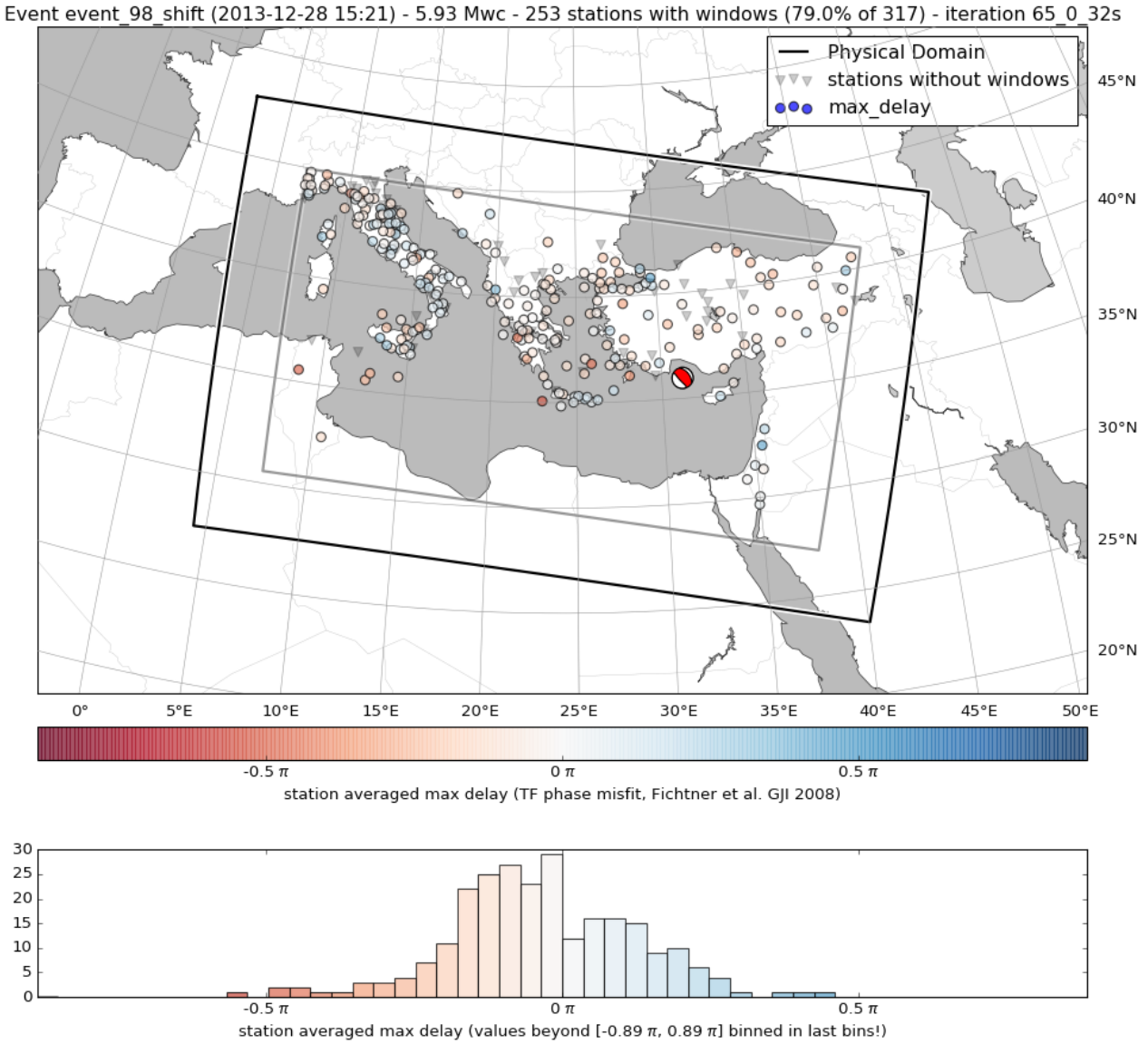

Figure 7: Distribution of "max delay" phase shifts for event 98 at iteration 65 (32–150 s) after shifting the event location towards the north-east (latitude + 0.15°, longitude + 0.25°).

Event 101

Event 101 fairly consistently showed synthetic waveforms arriving ahead of their corresponding observed data waveforms (Figure 8). This is confirmed by the spatial distribution and histogram of phase shifts, as demonstrated in Figure 9, where the histogram is skewed towards positive phase shifts (i.e. synthetics ahead of observed data). A time shift of 1 second was applied to remove this static shift. As a result, the spatial pattern of phase shifts centred around zero (Figure 3).

As with event 33, a time shift is not the only way in which the shift can be explained; however, for the purposes of the inversion (and given the additional constraints given by other events in the area) it is the easiest and most workable explanation.

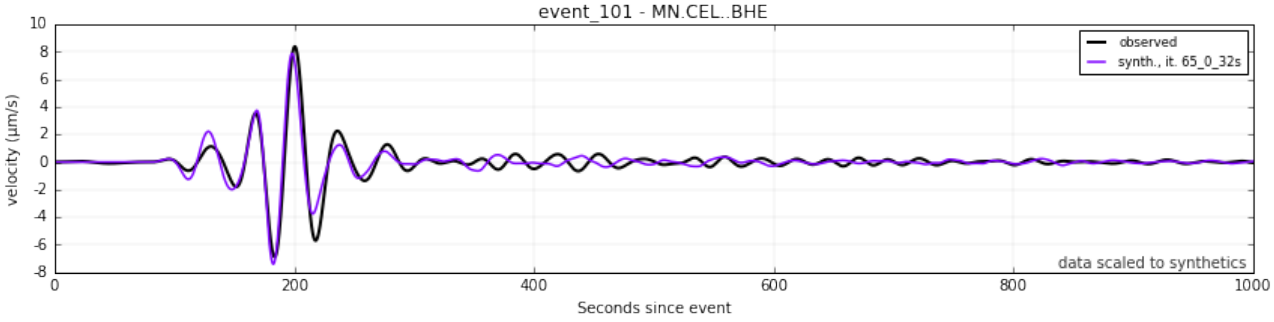

(a) Station MN.CEL (E component).

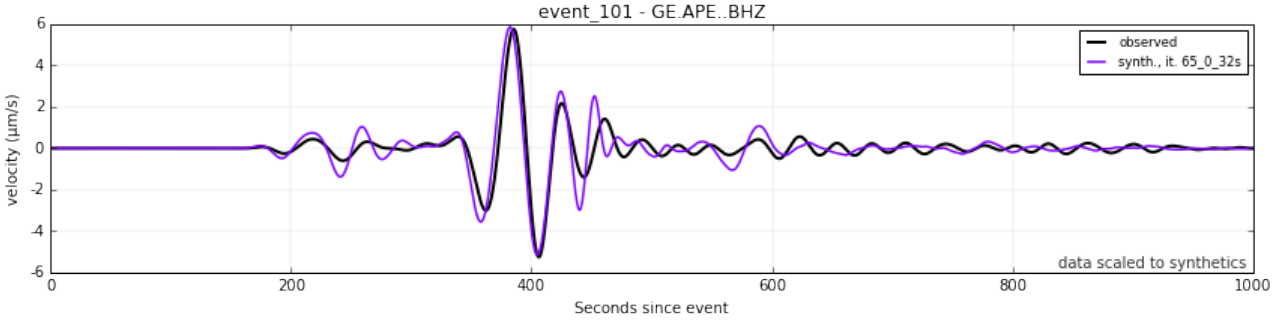

(b) Station GE.APE (Z component).

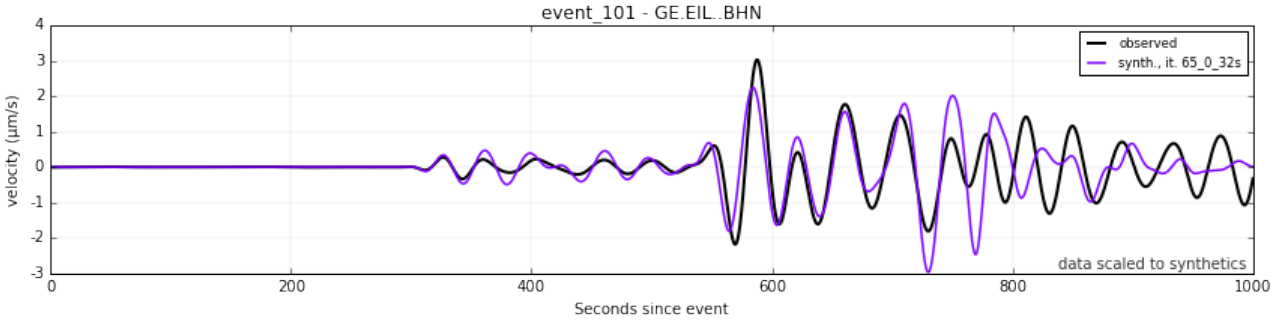

(c) Station GE.EIL (N component).

Figure 8: Seismograms for event 101 (uncorrected) and iteration 65_0_32s (32–150 s).

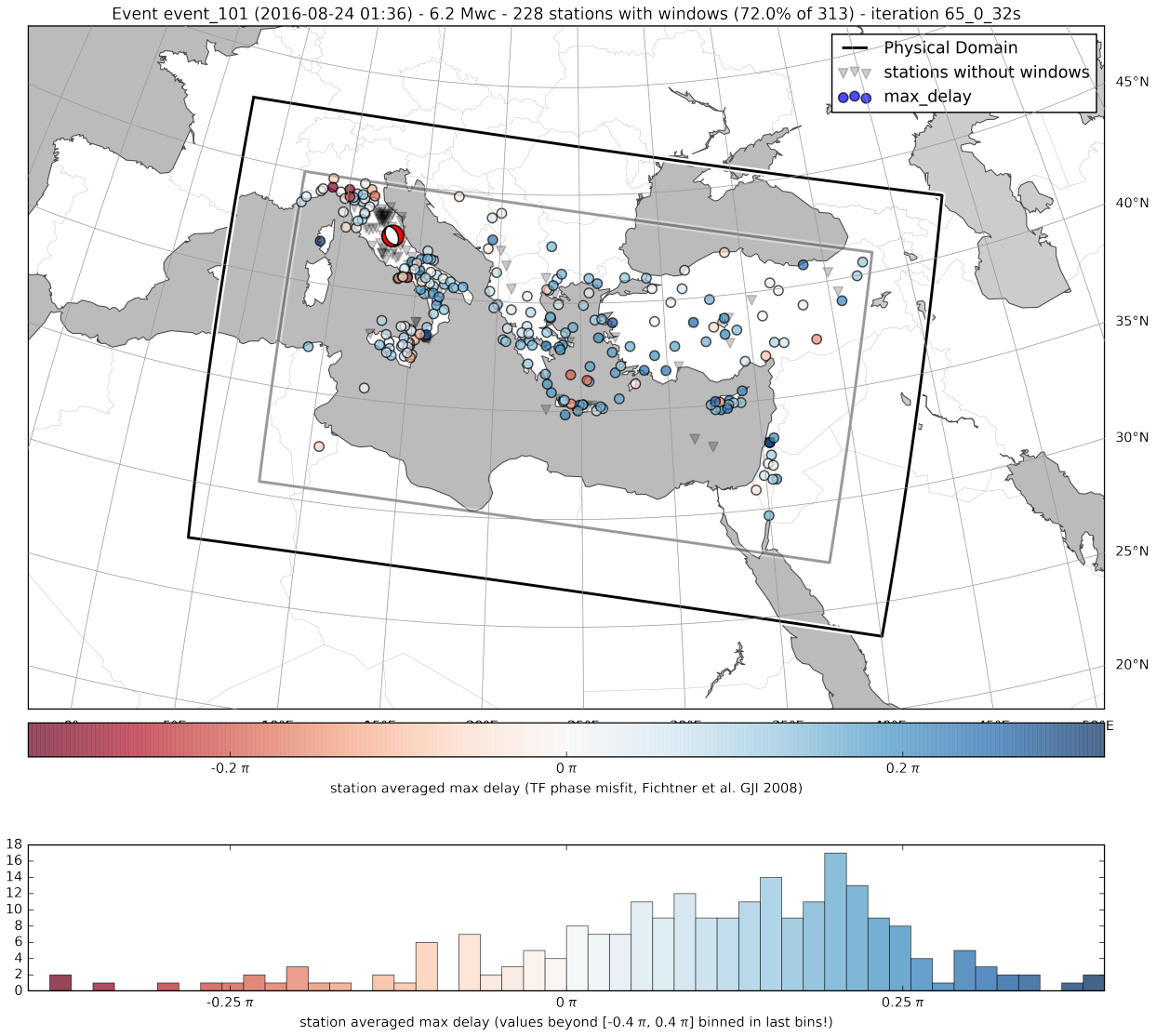

Figure 9: Original distribution of "max delay" phase shifts for event 101 at iteration 65_0_32s (32–150 s). This value is computed for each window as $\max(W_p\,(\phi - \phi_{\text{obs.}}))$ – see Equation 2 in the manuscript.

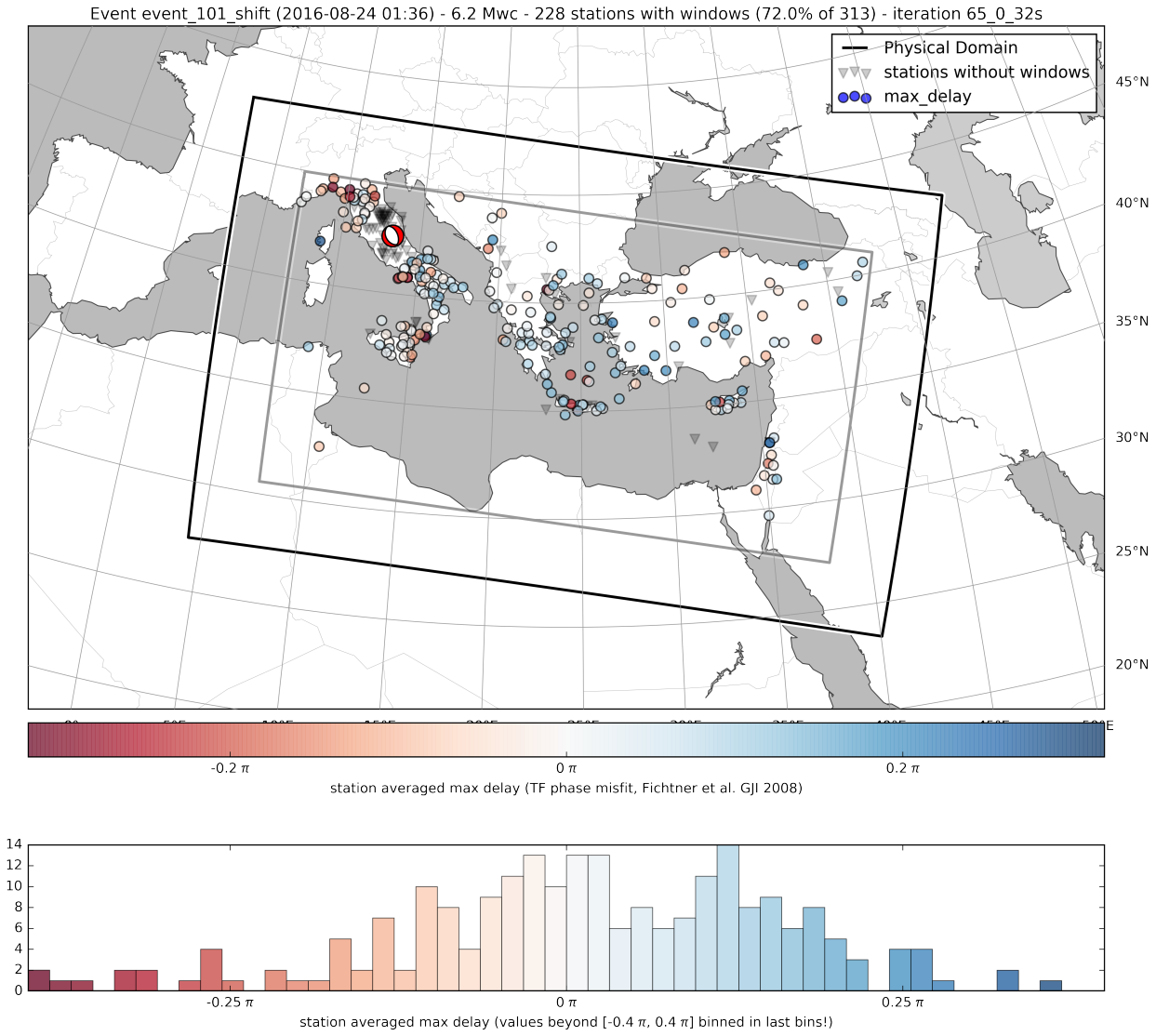

Figure 10: Distribution of "max delay" phase shifts for event 101 at iteration 65_0_32s (32–150 s) after shifting the event origin time by 1 second forward.

3 Processing of model updates

In order to compute a model update, the raw gradients for each model parameter are preprocessed before a descent direction is computed. This is done in order to improve convergence properties of the gradients. Kernels for each event are clipped at the 99th percentile in order to avoid too-strong localisation of updates especially in the source region, and then summed to produce the misfit gradient. The side and bottom edges are set to zero to remove potential boundary effects, and some smoothing is applied. This processing routine is based on experience from previous inversions and some initial experimentation, and the chosen parameters, re-evaluated for every set of iterations, are given in Table 2.

Additionally, at the end of certain sets of iterations, the cumulative model update is processed. These processing parameters are given in italics as the "Post-run" values in Table 2.

#	Period range	Frequency band	Number of iterations	Simulation length	Processing
0	100–150 s	0.0067–0.01 Hz	10	1200 s	cut 3°, 100 km; n_{sm}^{hv}=10
					Post-run: cut 4.5°, 350 km; n_{sm}^{h}=10, n_{sm}^{v}=50
1	80–150 s	0.0067–0.0125 Hz	10	1200 s	cut 3°, 100 km; n_{sm}^{hv}=10
					Post-run: cut 4.5°, 370 km; n_{sm}^{h}=3, n_{sm}^{v}=5
2	65–150 s	0.0067–0.0154 Hz	10	1200 s	cut 4.5°, 370 km; n_{sm}^{hv}=10
3	55–150 s	0.0067–0.0182 Hz	10	1001 s	cut 3°, 100 km; n_{sm}^{hv}=10
					Post-run: cut 2.5°, 320 km; n_{sm}^{h}=1, n_{sm}^{v}=3
4	46–150 s	0.0067–0.0217 Hz	10	990 s	cut 2°, 300 km; n_{sm}^{hv}=8
5	38–150 s	0.0067–0.0263 Hz	10	990 s	cut 2°, 300 km; n_{sm}^{hv}=8
					Post-run: density only: n_{sm}^{h}=10, n_{sm}^{v}=35
	38–150 s	0.0067–0.0263 Hz	5	990 s	cut 2°, 300 km; n_{sm}^{h}=3, n_{sm}^{v}=15
					density: n_{sm}^{h}=7, n_{sm}^{v}=60
6	32–150 s	0.0067–0.0313 Hz	15	1000 s	cut 2°, 300 km; n_{sm}^{h}=3, n_{sm}^{v}=15
					density: n_{sm}^{h}=7, n_{sm}^{v}=60
	32–150 s	0.0067–0.0313 Hz	5	1000 s	cut 2°, 300 km; n_{sm}^{h}=2, n_{sm}^{v}=10
					density: n_{sm}^{h}=4, n_{sm}^{v}=20
7	28–150 s	0.0067–0.0357 Hz	15	900 s	cut 2°, 300 km; n_{sm}^{h}=2, n_{sm}^{v}=10
					density: n_{sm}^{h}=4, n_{sm}^{v}=20

Table 2: Overview of inversion choices. The column 'Simulation length' shows the duration of each synthetic earthquake simulation. As frequency increases, the surface wave train becomes more compact (see Figure 3 in the manuscript), so the simulation duration can be shortened. The column 'Processing' indicates the processing applied to the gradients. 'Cut' indicates over which distance the model update is set to zero at the sides (in degrees) or the bottom (in km). This is in order to remove boundary reflection issues. 'n_{sm}' indicates the number of smoothing iterations applied, where superscripts h, v and hv indicate whether this is done in the horizontal direction, in the vertical direction, or simultaneously in the horizontal and vertical directions. In some iterations, additional smoothing was carried out to compensate for smoothing set to values that turned out to be too low. This is indicated in italics. After the first five period bands, separate smoothing for density is introduced, in order to avoid the accumulation of unphysical density values.

References

Dziewonski, A. M., Chou, T.-A., and Woodhouse, J. H. (1981). Determination of earthquake source parameters from waveform data for studies of global and regional seismicity. *Journal of Geophysical Research: Solid Earth*, 86(B4):2825–2852.

Ekström, G., Nettles, M., and Dziewonski, A. M. (2012). The global CMT project 2004-2010: centroid moment tensors for 13,017 earthquakes. *Phys. Earth Planet. Inter.*, 200-201:1–9.

Engdahl, E. R., van der Hilst, R., and Buland, R. (1998). Global teleseismic earthquake relocation with improved travel times and procedures for depth determination. *Bulletin of the Seismological Society of America*, 88(3):722–743.

Weston, J., Engdahl, E. R., Harris, J., DiGiacomo, D., and Storchak, D. A. (2018). ISC-EHB: reconstruction of a robust earthquake data set. *Geophysical Journal International*, 214(1):474–484.